

## **The redox reactions of strong inorganic oxidants: kinetics and mechanism**

### *OTKA final report*

#### **1. Introduction**

The expertise of our research group in solution phase reaction kinetics, as well as in the synthesis and characterization of functionalized aerogels has served as a basis for this project. During the last three decades, we have intensively studied complex redox reactions and developed comprehensive mechanisms for these reactive systems. Our earlier studies have uncovered a great number of challenging problems related to the redox chemistry of strong inorganic oxidants. We have also demonstrated that the boundaries of this research field can significantly be extended both in terms of research topics and methodology. We have realized that the kinetic approach used for investigating homogeneous reactions can also efficiently be utilized in heterogeneous systems. This concept has expanded the scope of our studies on functionalized aerogels.

Our primary goal was to elucidate the intimate details of selected redox reactions of strong inorganic oxidants, which are of utmost importance in environmental chemistry, biological systems, and industrial processes. We also wanted to explore how the scope of reaction kinetic research can be broadened in these systems. Dedicated studies on the properties of functionalized aerogels have been designed to clarify how the methodologies used in homogeneous reactions can be expanded to provide detailed interpretation of various phenomena in heterogeneous systems. In summary, our exploratory research was expected to resolve some of the discrepancies found in the literature, to lead to thorough interpretation of complex kinetic phenomena, and provide deeper understanding of specific features of functionalized aerogels.

As expected, most of the studied systems exhibit complex chemical phenomena that required the use of comprehensive experimental and evaluation protocols. In several cases, unexpected observations required the modification of the original research plan. Nevertheless, the main objectives of the project have been achieved. Most of the new results induced further studies, which are in progress in our research group.

## **2. Methods**

In order to obtain a comprehensive description of the studied systems, the experiments were carried out under a wide variety of experimental conditions. These studies required the combination of numerous complementary experimental and evaluation techniques. The analytical methods used for quantitative analysis of the reactants and products as well as for the identification of the intermediates included potentiometry, UV-VIS spectrophotometry, circular dichroism (CD) spectroscopy, HPLC, ionchromatography, CE-MS,  $^1\text{H}$  and  $^{13}\text{C}$  NMR spectroscopy,  $^1\text{H}$  NMR relaxometry, EPR spectroscopy, mass spectrometry.

The studied reactions proceed at different time scales that require the use of classical spectrophotometric, simple two component mixing and sequential stopped flow methods. Whenever it was possible, we applied pseudo-first-order approach to obtain preliminary information on the kinetics of the studied reaction. Often, the number of the absorbing species was determined by using dedicated linear algebraic analysis of the time resolved spectra recorded at different concentration ratios of the reactants. Finally, all experimental data were evaluated simultaneously by considering advanced kinetic models. Numerical algorithms were used to solve the corresponding differential equation systems and the parameters were estimated by non-linear least square fitting procedures. Theoretical calculations were also carried out to support some of the experimental conclusions.

The functionalized aerogels were synthesized by the classical sol – gel process. First, the solutions of the precursors were mixed to form the alcogel, which was allowed to age for an extended period of time. Subsequently, the solvent was replaced in the gel by acetone in an elaborated multi-step washing process. Finally, the aerogel was dried in a custom-made high-pressure reactor using supercritical carbon dioxide. The products were characterized using  $\text{N}_2$  porosimetry, scanning electron microscopy (SEM, LVSEM), dynamic light scattering (DLS), zeta potential analysis.

## **3. Results**

1. *N*-chloro-amino acids are readily formed in chlorination water treatment technologies. The corresponding reactions are also important in biological systems where HOCl plays a crucial role in the defense mechanism against invading pathogens. The intermediates and the products formed are of primary concern because they may have significant biological activities. In order to clarify intimate details and resolve the discrepancies in earlier results, the decomposition kinetics of *N*-chloro- $\alpha$ -alanine (MCA) was studied in the neutral –

alkaline pH range by UV–vis spectrophotometry and  $^1\text{H-NMR}$  method. In contrast to earlier reports, we have shown that the decomposition reaction proceeds via two distinct reaction paths:  $k_{\text{obs}} = k_{\text{OH}}[\text{OH}^-] + k$ . In slightly alkaline solution, the sole product is acetaldehyde. Under alkaline conditions, the main product is pyruvate ion, however, *N*-acetyl- $\alpha$ -alanine is also formed in a subsequent reaction sequence. A detailed kinetic model has been postulated that involves the rate determining dissociation of MCA into  $\text{Cl}^-$  ethanimine, which produces acetaldehyde in further reaction steps. Via the  $\text{OH}^-$  assisted path, first a carbanion is formed which undergoes dechlorination and produces iminopropionate ion. This species is transformed into pyruvate ion through hydration and deamination steps.

2. We have studied the formation of 17 *N*-chloramines from proteinogenic amino acids and  $\text{HOCl}$  by direct kinetic method in the pH 3.0 – 13.0 range. Thus, the uncertainties associated with the indirect methods used in some of the previous studies were eliminated. Each reaction proceeds according to an overall second order kinetics:  $v = -k [\text{HOCl}][\text{R-NH}_2]$  and the rate constants are several times  $10^7 \text{ M}^{-1}\text{s}^{-1}$ . A very slight correlation was found between the  $\lg k$  and the  $\text{p}K_{\text{AA}}$  (the  $\text{p}K$  of the amino group) of the amino acids. The results make possible to predict the reactivity order of the amino acids toward  $\text{HOCl}$  under various conditions. A comparison of the parameters of activation indicates that the presence of a bulky substituent on the side chain close to the  $\alpha$ -carbon atom decreases the strength of bonding between the reactants and make the structure more diffuse in the transition state. The chlorination of histidine proceeds via two pH dependent paths presumably leading to the formation of *N*-chloramine and a side chain chlorinated product. The latter compound may be involved in fast subsequent trans-chlorination reactions. The results resolve earlier discrepancies in the literature and are relevant in chlorination water treatment technologies as well as in the interpretation of *in vivo* processes involving the formation of *N*-chloro amino acids in a wide pH range.
3. The decomposition kinetics of the *N*-chloro derivatives of branched chain amino acids (BCAAs) – leucine, isoleucine, valine – have been studied in the neutral – alkaline pH range. On the basis of spectrophotometric measurements, we have confirmed that the decomposition proceeds via a spontaneous and an  $\text{OH}^-$  assisted path in each case:  $k_{\text{obs}} = k + k^{\text{OH}}[\text{OH}^-]$ . In this respect, these reactions show analogy to the decomposition of *N*-chloro- $\alpha$ -alanine.  $^1\text{H}$ ,  $^{13}\text{C}$  NMR and MS experiments were also performed to identify the

products and to monitor the progress of the reactions. It was established that the pH independent and the  $[\text{OH}^-]$  dependent paths lead to the formation of the same aldehyde in each system (isovaleraldehyde, 2-methyl-butylaldehyde, and isobutylaldehyde) as a primary product. This indicates a markedly different behavior compared to *N*-chloro- $\alpha$ -alanine. Under alkaline conditions, a portion of the aldehydes is converted into the corresponding Schiff-bases by the excess amino acid in a reversible process. We have proposed a common mechanism for these reactions that postulates the formation of imines and hemiaminals as reactive intermediates.

4. We have inspected how *N*-methylation affects the reactivity of selected amino acids in the chlorination reaction with HOCl at amino acid excess. It was shown that the *N*-chloro-*N*-methyl amino acids form in fast second-order reactions between *N*-methyl amino acids and hypochlorous acid. The comparison of the activation parameters for the reactions of *N*-methyl substituted and non-substituted branched-chain amino acids reveals that the transition-state features less organized structure and stronger bonds between the reactants in the reactions with the *N*-methyl derivatives. This is due to a combined positive inductive effect of the *N*-methyl group and the alkyl side chain as well as to the steric effects of the substituents. *N*-Methyl-*N*-chloro amino acids decompose much faster than the non-substituted compounds. The reaction rates do not depend on the pH, and the same final product is formed in the entire pH range. *N*-chlorosarcosine is an exception, as it decomposes via competing paths,  $k_d^{\text{obs}} = k_d + k_d^{\text{OH}}[\text{OH}^-]$ , yielding different final products. This feature is most likely due to the lack of an alkyl substituent on the  $\alpha$ -carbon atom. Under physiological pH, aldehydes and methylamine form in these reactions, which are not particularly toxic.
5. Monochloramine forms as an intermediate in water treatment technologies and it is an important secondary disinfecting agent. Nevertheless, only limited information is available on its basic chemical properties. We have explored the kinetics and mechanism of the decomposition of monochloramine in acidic aqueous solution. Fast kinetic measurements have convincingly showed that the formation of dichloramine via the disproportion of monochloramine is relatively fast and can be studied without any interference from side reactions. The reaction follows second-order kinetics and the main path is the reaction between the protonated and non-protonated forms of monochloramine. *Ab initio* molecular dynamics computations have provided the free energy profile in accord with the proposed

kinetic model and suggested that the reaction progresses via a short-lived chlorine-bridged intermediate which yields dichloroamine and ammonium ion through a deprotonation-coupled chlorine shift.

6. The removal of organic pollutants presents a major challenge for drinking water treatment plants. The chemical oxygen demand (COD) is essentially the measure of oxidizable organic matter in source waters. We have confirmed that COD can efficiently be decreased by adding Fe(II)/Fe(III) and sulfite ion to the source water while purging it with air. In this process, oxygen is activated to oxidize the main constituents of COD, i.e. organic substrates, via the generation of reactive inorganic oxysulfur radical ions. In the end, the total amount of sulfur (IV) is converted to the non-toxic sulfate ion. We have explored how the COD removal efficiency depends on the concentration of S(IV), the total concentration of iron species, the concentration ratio of Fe(II) and Fe(III), the purging rate and the contact time by using source water from a specific location (Királyhegyes, Hungary). The process has been optimized by applying the Response Surface Methodology (RSM). Under optimum conditions, the predicted and experimentally found COD removal efficiencies are in excellent agreement: 85.4% and 87.5%, respectively. It was demonstrated that the method is universally applicable because a remarkable decrease was achieved in COD, 62.0 – 88.5%, with source waters of various compositions acquired from 9 wells at other locations using the same conditions as in the case of Királyhegyes.
7. In order to gain insight into the chemical features of NiSOD enzymes, the complex formation reactions of the nickel binding loop in NiSOD and its related fragments have thoroughly been studied in the acidic – alkaline pH range. The *N*-terminally free and protected nonapeptides HCDLPCGVY-NH<sub>2</sub> (NiSODM1), HCDLACGVY-NH<sub>2</sub> (NiSODM3), and Ac-HCDLPCGVY-NH<sub>2</sub> (NiSODM2) and the *N*-terminally shortened analogues HCDL-NH<sub>2</sub> and HCA-NH<sub>2</sub> were synthesized, and their nickel(II) complexes have been studied by potentiometric and several spectroscopic techniques. EPR spectroscopy was also used to assign the coordinating donor sites after the in situ oxidation of nickel(II) complexes. The terminal amino groups are the primary metal binding sites for nickel(II) ion in NiSODM1 and NiSODM3, resulting in the high nickel(II) binding affinity of this peptide via the formation of a square-planar, (NH<sub>2</sub>, N<sup>-</sup>, S<sup>-</sup>, S<sup>-</sup>) or (NH<sub>2</sub>, N<sub>im</sub>, N<sup>-</sup>, S<sup>-</sup>) coordinated species in a wide pH range. The latter coordination sphere prevents the formation of the active structure of NiSOD under physiological pH. In situ oxidation of

the Ni(II) complexes yielded Ni(III) transient species in the case of nonapeptides. The square-pyramidal coordination environment with axial imidazole ligation provides the active structure of the oxidized form of NiSOD in the case of *N*-terminally free peptides. Consequently, these ligands are promising candidates for modeling NiSOD.

8. We have described the equilibria and detailed spectroscopic features of the zinc(II) complexes formed with the NiSOD binding loop and its related model fragments in the 4.0 – 11.0 pH-range. The zinc(II) complexes of L1 (HCDLPCGVY-NH<sub>2</sub>), L2 (Ac-HCDLPCGVY-NH<sub>2</sub>) and L3 (HCDLACGVY-NH<sub>2</sub>), as well as, the nickel(II) and zinc(II) complexes of L4 (HCDLPCG-NH<sub>2</sub>) have been studied by pH-potentiometric and several spectroscopic methods. We have concluded that the macrochelate coordinated zinc(II) complexes are dominant in the whole pH-range and the side chain donors of the peptides are involved in the metal binding. Therefore, the deprotonation and coordination of the peptide backbone occur only in a strongly alkaline solution. The acetylation of the peptide amino terminus (L2) significantly enhances the zinc(II) binding ability compared to the corresponding nickel(II) complexes. The complexes formed with zinc(II) and L2 are 2 – 3 orders of magnitude more stable than the corresponding nickel(II) complexes. This effect clearly shows the crucial role of the terminal amino group in the nickel binding of the NiSOD enzyme.
9. We have performed detailed equilibrium, spectroscopic and superoxide dismutase (SOD) activity studies on a nickel complex formed with a new metallopeptide bearing two nickel binding loops of NiSOD. The metallopeptide exhibits unique nickel binding ability and the binuclear complex is a major species with  $2 \times (\text{NH}_2, \text{N}^-, \text{S}^-, \text{S}^-)$  donor set even in an equimolar solution of the metal ion and the ligand. Nickel(III) species were generated by oxidizing the Ni<sup>II</sup> complexes with KO<sub>2</sub> and the coordination modes were identified by EPR spectroscopy. The binuclear complex formed with the binding motifs exhibits superior SOD activity, in this respect it is an excellent model of the native NiSOD enzyme. A detailed kinetic model is postulated that incorporates spontaneous decomposition of the superoxide ion, the dismutation cycle and fast redox degradation of the binuclear complex. The latter process leads to the elimination of the SOD activity. A unique feature of this system is that the Ni<sup>III</sup> form of the catalyst rapidly accumulates in the dismutation cycle and simultaneously the Ni<sup>II</sup> form becomes a minor species.

10. We have carried out a detailed SOD activity study on the nickel(II) complexes formed with the N-terminally free HHDLP<sub>CGVY</sub>-NH<sub>2</sub> (NiSODHH) and HCDLP<sub>HGVY</sub>-NH<sub>2</sub> (NiSODHC) peptides which were expected to mimick the nickel binding loop in the NiSOD enzyme. Cysteine was incorporated in different positions in these model peptides in order to gain better understanding the role of the cysteine residues in these systems. The results have been compared with those obtained with the wild-type fragment of NiSOD. The complex formation equilibria of nickel(II) with the two peptides exhibit different features. In the case of NiSODHH, the ligand field of the (NH<sub>2</sub>, N<sub>Im</sub>, N<sub>Im</sub>, S<sup>-</sup>) donor set is not strong enough to cause spin pairing and an octahedral paramagnetic complex is formed under physiological conditions. In contrast, NiSODHC forms a square-planar diamagnetic complex with (NH<sub>2</sub>, N<sup>-</sup>, S<sup>-</sup>, N<sub>Im</sub>) donors, which exhibits remarkable SOD activity. Our results unambiguously prove that the presence of cysteine in the secondary position of the peptide chain is crucial to establish the square-planar geometry in the reduced form of NiSOD, while the distant cysteine affects the redox properties of the Ni(II)/Ni(III) couple. Compared to the model systems, the Ni(II) complex with the wild-type fragment of NiSOD exhibits superior SOD activity. This confirms that both cysteinyl residues are essential in the efficient degradation of superoxide ion. The enzyme mimetic complexes are also capable of assisting the decomposition of superoxide ion; however, they show considerably smaller catalytic activity due to the absence of one of the cysteine residues.
11. We have designed a novel metallopeptide mimicking the binding loop of nickel containing SOD enzyme (NiSOD). D-Penicillamine, a natural decomposition product of penicillin, was introduced into the peptide chain yielding the H(Pen)DLPCGLY (wtPen) peptide. The nickel(II) binding ability of wtPen was characterized by pH-potentiometry, spectroscopic (UV-Vis, CD, MS, NMR) and computational techniques (full DFT and Molecular Dynamics methods). Oxidation of the Ni(II) complex by KO<sub>2</sub> yields a square pyramidal Ni(III) species coordinated by the axial His-N in a well defined  $\alpha$ -helix folding state. The structure of the Ni(III) species was analyzed by EPR spectroscopy and theoretical methods confirming that the donor set involved in the metal ion coordination and the folding state are retained after oxidation. The complex exhibits superior SOD activity, which was studied by sequential stopped-flow method. Thorough analysis of the data shows that the Ni(III) species rapidly accumulates in the nickel catalyzed decomposition of superoxide anion. Accordingly, the presence of the penicillamine moiety close to the catalytic center increases the life-time of the Ni(III) transient species. In contrast, Ni(III) exists only at

relatively low concentration level in the dismutation reaction catalyzed by the native NiSOD enzyme fragment.

12. The relaxivity of Gd(HP-DO3A) (H3HP-DO3A = 10-(2-hydroxypropyl)-1,4,7,-10-tetraazacyclododecane-1,4,7-triacetic acid) was studied as a function of pH and buffer composition in order to identify the main factors of the observed relaxation enhancement due to the exchange of the coordinated hydroxyl proton. We have confirmed that the control of the p*K* of the coordinated alcoholic –OH moiety in the ligand is fundamental to utilize the proton exchange enhanced relaxivity under physio/pathologic conditions.
13. A current challenge in medical diagnostics is how to obtain high MRI relaxation enhancement using Gd<sup>III</sup>-based contrast agents containing the minimum concentration of Gd<sup>III</sup> ions. We have confirmed that in GdHPDO3A-like complexes a primary amide group located in close proximity to the coordinated hydroxyl group can provide a strong relaxivity enhancement at slightly acidic pH. A maximum relaxivity of  $r_1 = 9.8 \text{ mM}^{-1} \text{ s}^{-1}$  (20 MHz, 298 K) at acidic pH was achieved, which is more than double that of clinically approved MRI contrast agents under identical conditions. This effect was found to strongly depend on the number of amide protons, i.e. it decreases with a secondary amide group and almost completely vanishes with a tertiary amide. This relaxivity enhancement is attributed to an acid-catalyzed proton exchange process between the metal-coordinated OH group, the amide protons and second sphere water molecules. The mechanism and kinetics of the corresponding H<sup>+</sup> assisted exchange process are discussed in detail and a novel simultaneous double-site proton exchange mechanism is proposed. Furthermore, <sup>1</sup>H and <sup>17</sup>O NMR relaxometry, Chemical Exchange Saturation Transfer (CEST) on the corresponding Eu<sup>III</sup> complexes, and thermodynamic and kinetic features have also been studied. The results highlight the optimal physico-chemical properties required to achieve high relaxivity with this series of Gd<sup>III</sup> complexes. We have concluded that proton exchange provides an important opportunity to enhance the relaxivity of contrast agents, providing that labile protons close to the paramagnetic center exist.
14. We have systematically studied the kinetics and mechanism of the *cis* dihydroxylation of *cis*-1,2-dichloroethylene, *trans*-1,2-dichloroethylene, and trichloroethylene by osmium tetroxide in aqueous solution. The stoichiometry of the process has been determined by utilizing the principle of continuous variation of reactant ratios with spectrophotometric detection. The results always confirmed 1:1 stoichiometry, which is in agreement with



dihydroxylation. All three reactions were found to proceed in two distinct steps. The first step occurred on a time scale of seconds and was associated with a minor change in absorbance and was identified as the formation of a 1:1 adduct between the two reagents. It is the osmium(VI) ester that plays a decisive role in catalytic applications. This species is formed in an equilibrium that is very much shifted toward the reactants, so the osmium(VI) complex is detectable kinetically, but its concentration is never high enough for structural characterization. The second reaction is accompanied by major spectral changes; and involves the formation of the final products. Our results clearly show that it is possible to detect the intermediate of the process by careful kinetic studies. It is also possible that the same strategy might be successful in other  $\text{OsO}_4$ -dependent dihydroxylation processes.

15. We have carried out theoretical calculations to emulate the visible region of the electronic absorption spectra of Cu(II) complexes on the basis of time-dependent density functional theory (TD-DFT). The performance of twelve functionals for the prediction of absorption maxima ( $\lambda_{\text{max}}$ ) was tested with eleven compounds of different geometry, donor groups and charge. The ranking of the functionals for  $\lambda_{\text{max}}$  was determined in terms of mean absolute percent deviation (MAPD) and standard deviation (SD) as follows: BHandHLYP > M06 >> CAM-B3LYP >> MPW1PW91 ~ B1LYP ~ BLYP > HSE06 ~ B3LYP > B3P86 ~  $\omega$ -B97x-D >> TPSSh >> M06-2X (MAPD) and BHandHLYP > M06 ~ HSE06 >  $\omega$ -B97x-D ~ CAM-B3LYP ~ MPW1PW91 > B1LYP ~ B3LYP > B3P86 > BLYP >> TPSSh >> M06-2X (SD). The protocol validated in the first step was applied to i) calculate the number of transitions in the spectra and relate them to the geometry of Cu(II) species; ii) determine the coordination of axial water(s); iii) predict the electronic spectra of the systems where Cu(II) is bound to human serum albumin (HSA) and to the regions 94–97 and 108–112 of prion protein (PrP). The results indicate that the proposed computational protocol allows a successful prediction of the electronic spectra of Cu(II) species and to relate an experimental spectrum to a specific structure.
16. *N*-oxides of *N*-heteroaromatic compounds find widespread applications in various fields of chemistry. Although the strictly planar aromatic structure of 1,10-phenanthroline (phen) is expected to induce unique features of the corresponding *N*-oxides, the potential of these compounds has not been explored. In fact, appropriate procedure has not been reported for synthesizing these derivatives of phen before. We have provided a straightforward method

for the synthesis of a series of mono-*N*-oxides of 1,10-phenanthrolines. The parent compounds were oxidized by a green oxidant, peroxomonosulfate ion in acidic aqueous solution. The products were obtained in high quality and at good to excellent yields. Our systematic study reveals a clear-cut correlation between the basicity of the compounds and the electronic effects of the substituents on the aromatic ring. The UV spectra of these compounds were predicted by DFT calculations at the TD-DFT/TPSSh/def2-TZVP level of theory.

17. Based on time resolved dynamic light scattering (DLS) and UV–vis spectrometric experiments, we have proposed a simple kinetic model to describe the formation of TiO<sub>2</sub> particles up to the size of a few hundred nanometers in an aqueous suspension. It was confirmed that the turbidity (i.e., the apparent absorbance at 500 nm) of a stable TiO<sub>2</sub> suspension is proportional to the TiO<sub>2</sub> concentration at a constant particle size and proportional to the particle size at a constant titanium concentration. The kinetic model includes the following three steps: i) the rapid hydrolysis of the precursor provides primary particles for the subsequent steps; ii) relatively slow dimerization of the primary particles; iii) the formation of larger particles in the step-by-step addition of further primary units. The model provides an excellent fit to the experimental data. An integrated rate equation was derived which predicts the time-dependent mean particle size as the function of the initial precursor concentration well.
18. We have confirmed that supercritically dried, mesoporous silica-gelatin hybrid aerogels of 4 – 24 wt.% gelatin content show high selectivity for the adsorption of aqueous Hg(II) in the simultaneous presence of Cu(II), Cd(II), Co(II), Pb(II), Ni(II), Ag(I) and Zn(II). The aerogels have been characterized by SEM and N<sub>2</sub> porosimetry, and their aqueous particle size distributions and Zeta potentials have been reported. The adsorption properties of the hybrid aerogels have been studied as function of their composition, initial aqueous Hg(II) concentration, contact time and pH. The optimum pH for adsorption is 6.0, where the surface of the aerogel is already negatively charged, but Hg(II) does not completely hydrolyze. The Hg(II) uptake of the hybrid aerogels increases with increasing gelatin content and levels off at 24 wt.% gelatin. Gelatin provides the active sites for Hg(II) binding, thus higher gelatin content results in higher adsorption capacity. However, high gelatin content also induces the extensive swelling of backbone and the partial collapse of the open porous structure, which decreases the specific surface area. Washing the

equilibrated aerogels with a 2.5 mM solution of EDTA complexing agent quantitatively liberates bound Hg(II). The regenerated aerogels demonstrate practically intact adsorption capacities in 5 cycles of reuse. Coordination chemical considerations reveal that Hg(II) is selectively complexed by the soft Lewis-base side chains of collagen.

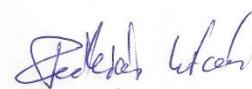
19. Mesoporous aerogel microparticles are promising drug delivery systems, however, their *in vivo* biodistribution pathways and health effects are unknown. We have investigated the biological impact of these materials *in vivo* experiments. Suspensions of fluorescein-labeled silica–gelatin hybrid aerogel microparticles were injected into the peritoneum (abdominal cavity) of healthy mice in concentrations of 52 and 104 mg kg<sup>-1</sup> in a 3-week-long acute toxicity experiment. No physiological dysfunctions were detected, and all mice were healthy. An autopsy revealed that the aerogel microparticles were not present at the site of injection in the abdominal cavity at the end of the experiment. The histological study of the liver, spleen, kidneys, thymus and lymphatic tissues showed no signs of toxicity. The localization of the aerogel microparticles in the organs was studied by fluorescence microscopy. Aerogel microparticles were not detected in any of the abdominal organs, but they were clearly visible in the cortical part of the parathymic lymph nodes, where they accumulated. This observation in combination with the absence of microparticles in the reticuloendothelial system organs, such as the liver or spleen, suggests that the microparticles entered the lymphatic circulation. This biodistribution pathway could be exploited to design passive targeting drug delivery systems for flooding metastatic pathways of abdominal cancers that spread via the lymphatic circulation.
20. We have investigated how static supercritical fluid extraction can be used to concentrate the aroma materials of common herbs and spices. The technique has provided a higher number of components and cleaner extract than the one-step ethanol maceration. The one-step supercritical fluid extraction of the aroma compounds has been combined with their *in situ* adsorption in hydrophilic and hydrophobic silica aerogels. The extracts have been analyzed by GC–MS technique and 55 aroma compounds have been identified. Most of the compounds have been adsorbed in both polar and apolar silica aerogels and no direct correlation could be established with the surface polarity. However, previously undetected compounds enriched to an analytically significant level, while others competed with each other for the active sites on the surface. We have demonstrated that functionalized silica aerogels can be used as a new type of aroma storage materials and as selective and tunable

adsorbents for the extraction and enrichment of potentially active components from a complex matrix.

21. The imaging of non-conducting materials by scanning electron microscopy (SEM) is most often performed after depositing few nanometers thick conductive layers on the samples. We have shown that even a 5 nm thick sputtered gold layer can dramatically alter the morphology and the surface structure of many different types of aerogels. Silica, polyimide, polyamide, calcium-alginate and cellulose aerogels were imaged in their pristine forms and after gold sputtering utilizing low voltage scanning electron microscopy (LVSEM) in order to reduce charging effects. The morphological features seen in the SEM images of the pristine samples are in excellent agreement with the structural parameters of the aerogels measured by nitrogen adsorption-desorption porosimetry. In contrast, the morphologies of the sputter coated samples are significantly distorted and feature nanostructured gold. These findings confirm that extra care should be taken in order to ensure that gold sputtering does not cause morphological artifacts. Otherwise, the application of low voltage scanning electron microscopy is preferred because it yields high resolution images of pristine non-conducting aerogels.

These results have been reported in 22 papers in internationally renowned journals (21 Q1, 1 Q2, 1 Q3 and IF = 124.9). In the first period of the project, the results were also presented in international and national conferences. Eventually, this activity has ceased due to the COVID situation.

Debrecen, January 31, 2022.



Dr. István Fábán

principal investigator